ELECTRONIC EQUILIBRIUM AS A FUNCTION OF DEPTH IN TISSUE FROM COBALT-60 POINT SOURCE EXPOSURES

A Thesis

by

JO ANN MYRICK

Submitted to the Office of Graduate Studies of
Texas A&M University
in partial fulfillment of the requirements for the degree of

MASTER OF SCIENCE

August 1994

Major Subject: Health Physics

DISCLAIMER

ELECTRONIC EQUILIBRIUM AS A FUNCTION OF DEPTH IN TISSUE FROM COBALT-60 POINT SOURCE EXPOSURES

A Thesis

by

JO ANN MYRICK

Submitted to Texas A&M University
in partial fulfillment of the requirements
for the degree of

MASTER OF SCIENCE

Approved as to style and content by:

Warren D. Reece
(Chair of Committee)

John W. Poston, Sr.
(Member)

Michael Walker
(Member)

John W. Poston, Sr.
(Head of Department)

August 1994

Major Subject: Health Physics

ABSTRACT

Electronic Equilibrium as a Function of Depth in Tissue from Cobalt-60 Point Source Exposures. (August 1994)

Jo Ann Myrick, B.S., Texas A&M University

Chair of Advisory Committee: Dr. Warren D. Reece

The Nuclear Regulatory Commission has set the basic criteria for assessing skin dose stemming from hot particle contaminations. Compliance with 10 CFR 20.101 requires that exposure to the skin be evaluated over a 1 cm^2 area at a depth of 0.007 cm. Skin exposure can arise from both the beta and gamma components of radioactive particles and gamma radiation can contribute significantly to skin doses. The gamma component of dose increases dramatically when layers of protective clothing are interposed between the hot particle source and the skin, and in cases where the hot particle is large in comparison to the range of beta particles. Once the protective clothing layer is thicker than the maximum range of the beta particles, skin dose is due solely to gamma radiation.

Charged particle equilibrium is not established at shallow depths. The degree of electronic equilibrium establishment must be assessed for shallow doses to prevent the over-assessment of skin dose because conventional fluence-to-dose conversion factors are not applicable. To assess the effect of electronic equilibrium, selected thicknesses of tissue equivalent material were interposed between radiochromic dye film and a ^{60}Co hot particle source and dose was measured as a function of depth. These measured values were then compared to models which are used to calculate charged particle equilibrium. The Miller-

Reece model was found to agree closely with the experimental data while the Lantz-Lambert model overestimated dose at shallow depths.

DEDICATION

For my mother and my wonderful fiancé, Jerry, who believed in me even when I did not believe in myself and kept me going when I wanted to give up. I could not have made it without the two of you and I can never thank you enough. I love you!!!

ACKNOWLEDGMENTS

I would like to thank Dr. W. D. Reece for his guidance and encouragement during the duration of this work. I would also like to thank Dr. John W. Poston, Sr. and Dr. Michael Walker for their patience and support. Finally, I would like to express my gratitude to Mr. Joe Snook, Mr. Tom Fisher, and all of the other Nuclear Science Center employees who helped me make modifications and repairs to the scanning densitometer. This work was performed under appointment to the Applied Health Physics Fellowship Program administered by Oak Ridge Associated Universities for the U. S. Department of Energy.

TABLE OF CONTENTS

LIST OF FIGURES

LIST OF TABLES

CHAPTER I

INTRODUCTION

The Nuclear Regulatory Commission has provided the basic criteria for assessing skin contamination stemming from hot particles in IEN 86-23 (U. S. Nuclear Regulatory Commission 1986). Compliance with 10 CFR 20.101 requires that exposure to the skin be evaluated over a 1 cm^2 area at a depth of 0.007 cm (7 mg cm^{-2}) (As a note to the reader, SI units will be used but references will be quoted in the units given, i.e. centimeters). Both the beta and gamma components must be evaluated to determine the total exposure to the skin from radioactive particles.

Early efforts to model dose to the skin from hot particles ignored the self absorption of beta rays and the contribution to dose by gamma rays. Gamma radiation arising from exposure to large hot particles consisting primarily of activation products may contribute significantly to skin dose. By a large margin, the principal radionuclide in activation hot particles is ^{60}Co, and significant attenuation of the low-energy beta particles emitted by ^{60}Co can occur within the source material or within layers of protective clothing. Ordinarily, gamma radiation is not attenuated significantly by the source material or by protective clothing.

The dose arising from the beta particle component is relatively well understood.

This thesis follows the format of Health Physics.

Tables have been published that relate activity to dose rate and several computer codes that calculate these values are available (Traub et al, 1987) However, computer codes used to calculate the gamma component of skin dose may be incorrect. This is primarily because of the difficulty in assessing the degree of electronic equilibrium achieved. The initial interaction between a photon and an electron within the tissue results in the conversion of some of the photon energy to kinetic energy given to an orbital electron. It is these high speed secondary electrons that produce ionizations and excitations which break molecular bonds. Electronic equilibrium exists when the energy carried out of the volume of interest by charged particles is replaced by charged particles created by other photon interactions in the surrounding medium. Lantz and Lambert (1990) describe the necessity of a charged particle equilibrium (CPE) correction factor by discussing the mechanisms involved in photon energy transfer and absorption.

Energy absorption from a pure photon beam increases with depth in a material until a maximum value is reached. This maximum value is referred to as the equilibrium thickness. The equilibrium thickness is comparable to the range of the most energetic secondary electron created by the photon within the material, at which point equilibrium is established. The equilibrium thickness is both gamma energy and material dependent. The higher the gamma energy, the greater the equilibrium thickness. At shallow depths, calculated doses are higher than the actual dose delivered as charged particle equilibrium has not been established.

The gamma component of dose increases dramatically when layers of protective clothing, i.e. anti-contamination suits, are interposed between the hot particle source and

the skin. This leads to large errors if the gamma component is ignored. Once the protective clothing layer is thicker than the range of the beta particles, the skin dose is due solely to gamma radiation. However, the degree of electronic equilibrium established must be assessed for shallow doses to prevent the over-assessment of skin dose. A CPE correction factor should be developed to determine the actual contribution of the gamma component to skin dose from hot particles.

The primary goal of this research is the determination of charged particle equilibrium correction factors. Radiochromic dye film will be used to measure dose profiles from a ^{60}Co hot particle (1 mm activated stellite particle recovered from Palo Verde steam generators). A charged particle equilibrium thickness will be determined from these measurements and compared to the current CPE models.

CHAPTER II

THEORY

Absorbed Dose Theory

Exposure to radiation causes damage to cells and tissues of the body through energy deposition. This deposited energy causes ionization and excitation in the tissue, which alters the molecular structure, leading to cell damage. Radiation damage is approximately proportional to the specific absorbed energy in tissue. Formally, absorbed dose (D) is the energy imparted to matter through ionizations and excitations per unit mass of irradiated matter. The absorbed dose at any point in a given volume can be defined as:

$$D = \frac{d\varepsilon}{dm} \qquad (1)$$

where ε is the expected energy imparted in the finite volume during a given period of time.

The specific gamma ray constant, Γ, can be used to calculate dose arising from a point source in a nonattenuating medium. This constant is a combination of all the factors required to calculate the dose to a point at a specified distance from a particular radionuclide point source. There are many units for Γ, e.g., mSv m^2 MBq^{-1} h^{-1} (The Health Physics and Radiological Health Handbook 1992). Dose may be obtained in gray by dividing the specific gamma constant by the quality factor for gamma rays.

Equation 2 shows how dose is calculated using Γ:

$$D = \frac{\Gamma A_o}{r^2} \qquad (2)$$

where A_o is the activity of the point source and r^2 is the square of the distance from the source to the dose point.

Of course, this idealized method of dose calculation is fairly limited. Equation (2) is only valid for point sources, in nonattenuating media, and charged particle equilibrium conditions must exist, as discussed later. Other means for calculating dose must be used for different geometries such as disk or line sources and when charged particle equilibrium does not exist.

Charged Particle Equilibrium

For indirectly ionizing radiations, e.g. photons, dose is not necessarily directly related to fluence. Indirectly ionizing radiation deposits energy by creating secondary charged particles through interactions within the dose volume, e.g. Compton electrons are created by photons. However, eqn (2) can be applied if the energy carried away from the point of interaction is replaced by charged secondary particles created elsewhere in the medium. Formally, charged particle equilibrium (CPE) exists in a specified volume, *v*, if the energy carried away by charged particles produced in *v* is replaced by charged particles created in the surrounding medium. Figure 1 illustrates CPE conditions for an external radiation source. The larger volume, *V*, is uniformly irradiated by photons. These indirectly ionizing radiations interact in *V* producing secondary charged particles uniformly throughout. CPE will exist if the boundaries of *V* and the smaller internal volume *v* are

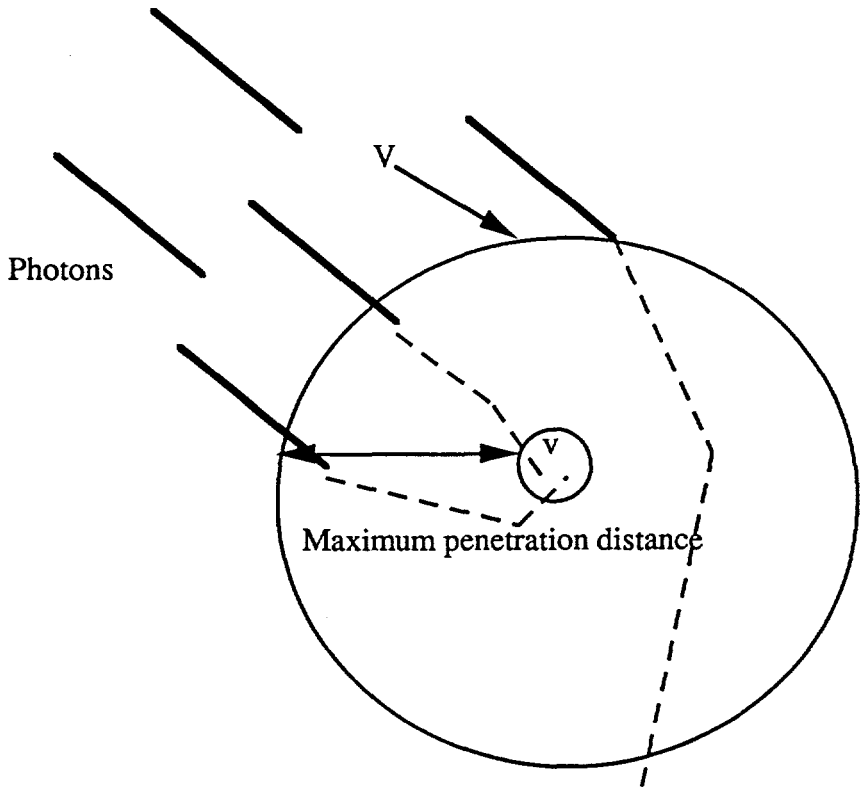

Fig. 1. CPE conditions for an external radiation source.

separated by at least the maximum penetration distance of the most energetic secondary charged particle present.

Under CPE conditions, the absorbed dose (D) is equal to the collision kerma (K_c). Collision kerma is defined as the expected net energy transferred to charged particles per unit mass at the point of interest (Attix 1986). Collision kerma excludes radiative energy losses and energy passed from one charged particle to another. This relationship is important because it equates the measurable quantity D with the calculated quantity K_c defined by eqn (3).

$$K_c = \Psi(\frac{\mu_{en}}{\rho}) \qquad (3)$$

The energy fluence, Ψ, is the average total energy carried by all particles or photons striking near a designated point. For monoenergetic photons, the energy fluence is defined as:

$$\Psi = \Phi E \qquad (4)$$

where E is the energy of the photons and Φ is the fluence. Fluence is the average number of particles passing near the point of interest and is expressed in units of photons cm^{-2}.

The mass energy-absorption coefficient, $\frac{\mu_{en}}{\rho}$, relates the fraction of the photon beam energy converted into dose deposited locally by charged particles. The mass energy-absorption coefficient is related to the mass energy-transfer coefficient by the following equation:

$$\frac{\mu_{en}}{\rho} = \frac{\mu_{tr}}{\rho}(1-g) \qquad (5)$$

where μ_{tr} is the mass-energy transfer coefficient and the average fraction of secondary electron energy lost in radiative interactions such as bremsstrahlung and inflight annihilation is g.

The mass-energy transfer coefficient is related to the linear absorption coefficient, μ_a in the following manner:

$$\mu_{tr} = \mu_a = f_c . \sigma \qquad (6)$$

where f_c is the fraction of photon energy transferred to electron kinetic energy in Compton collisions and σ is the Compton cross section. The contributions of pair production and the photoelectric effect are not considered in this case as their contributions are negligible. The transfer of photon energy to electron kinetic energy in the designated volume is accounted for by the mass energy-transfer coefficient, $\frac{\mu_{tr}}{\rho}$. This correction is made because even the low-energy bremsstrahlung photons are assumed to leave the volume of interest about the dose point.

Thus, for conditions in which charged particle equilibrium exists, absorbed dose can be predicted by:

$$D = \Phi E \frac{\mu_{en}}{\rho}. \qquad (7)$$

Dose rate can be calculated by substituting fluence rate, ϕ, for fluence where absorbed dose and dose rate can be related to collision kerma.

The same theory can be extended from beam geometry to cases in which a point source is irradiating a given volume. The fluence rate for a point source is defined as:

$$\phi(r)=\frac{S_p}{4\pi r^2} \tag{8}$$

where, S_p is the source strength and r is the distance from the source to the point irradiated. The dose rate due to a point source in CPE conditions is:

$$D=\frac{S_p}{4\pi r^2}E\frac{\mu_{en}}{\rho} \tag{9}$$

The dose rate cannot be calculated as easily when charged particle equilibrium does not exist. If the distance separating the boundaries of V and v is not greater than the maximum range of the charged particles, CPE may not exist. In cases where the CPE thickness does not separate the boundaries of the dose volumes, the fraction of charged particle equilibrium present must be determined, and this fractional CPE included in the dose equation (Lantz and Lambert 1990):

$$\mathrm{D}=(\mathrm{CPE\,fraction})\phi\mathrm{E}\frac{\mu_{en}}{\rho}. \tag{10}$$

The CPE fraction allows dose rate calculations to be performed when CPE does not exist by accounting for the fraction of CPE present at the point at which dose is being evaluated.

The absence of CPE is utilized in cancer therapy to limit the damage done to superficial tissues by the radiation beams used to destroy deep tumors. The skin and superficial tissues overlying the tumor are spared by choosing beam energies which will

reach CPE after a few millimeters travel through tissue. Tissues overlying the tumor do not receive the maximum dose because maximum dose is proportional to CPE fraction.

Literature Review

Chabot (1990) derived a CPE correction factor. Figure 2 presents a schematic of the dimensions of a point source irradiating a fixed area. The dose over the area of interest is:

$$\int_0^L \int_0^{2\pi} \frac{A\Gamma\, l\, dl\, d\theta}{R^2} \tag{11}$$

Integrating this equation and dividing by the total area yields the average dose:

$$D_{avg} = \frac{2\pi A\Gamma \ln \frac{\sqrt{H^2 + L^2}}{H}}{\pi L^2}. \tag{12}$$

For these equations, A is the activity of the point source and all other variables are as previously defined in the text and Fig. 2.

Chabot's model is based on the assumptions that secondary electrons produced by photon interactions move in a forward direction toward the dose point, the dose produced by these electrons decreases exponentially with the distance traveled in the media, and the dose due to the electrons decreases inversely with the square of the distance traveled from the point source. He also assumes that no bremsstrahlung radiation is produced by electron interactions. The dose attenuation coefficient for the secondary electrons is defined as υ_S.

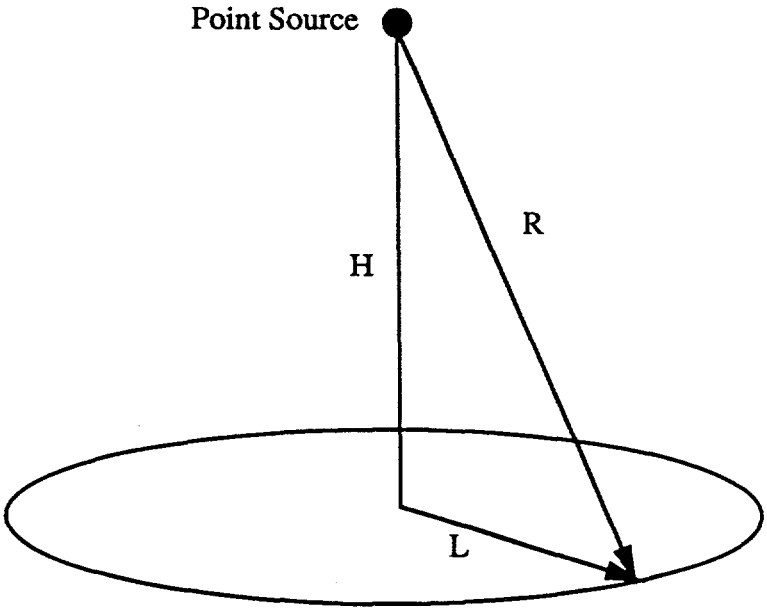

Figure 2. Point source irradiating a fixed area.

This parameter is then used to write an expression for the differential dose rate resulting from electrons produced at depth x and arriving at depth T:

$$dDe = \left(\frac{A\Gamma}{x^2}\right) \nu_S \, dx \, e^{-\nu_S (T-x)} \left(\frac{x}{T}\right)^2. \qquad (13)$$

Integrating eqn (11) for all values of x from 0 to T we obtain:

$$D_e = \left(\frac{A\Gamma}{T^2}\right)(1 - e^{-\nu_S T}). \qquad (14)$$

The first term is the dose rate under equilibrium conditions at distance T from an isotropic point source. The dose rate averaged over a fixed area can be calculated by replacing T with the variable t in eqn (12) and using the terms in Fig. 2 with t in place of x (eqn 15):

$$D = \int_{H}^{\sqrt{H^2+R^2}} \frac{A\Gamma}{t^2}\left(1 - e^{-\nu_s t}\right)\frac{2\pi t \, dt}{\pi L^2} \quad . \qquad (15)$$

Integrating eqn (15) yields:

$$D_{e,avg} = \frac{2\pi A\Gamma \ln\left(\frac{\sqrt{H^2 + L^2}}{H}\right) - \left(E_1(\nu_S H) - E_1\left(\nu_S \sqrt{H^2 + L^2}\right)\right)}{\pi L^2}. \qquad (16)$$

It can be seen, through a comparison of equations (15) and (11), that the lack of electronic equilibrium reduces the average dose rate by the difference of the two exponential integral functions in the second major term of eqn 16.

Chabot used unpublished medical therapy depth dose information to estimate the value of υ_S for secondary electrons. He used a modified form of Loevinger's (Hine and Brownell 1956) expression for beta emitters to approximate υ_S:

$$\nu_s = 13(E - 0.036)^{-1.37} \qquad (17)$$

where, E is the photon energy in MeV. This equation is valid for water and soft tissue. Chabot calculated υ_S for ^{60}Co on the skin surface as 10 cm^{-1}.

Lantz and Lambert used the ν_s value calculated by Chabot as the basis for their research (Lantz and Lambert 1990). Values of (1-dose fraction) were calculated and plotted. Figure 3 is a plot dose fraction as a function of depth in water. The data points were found to fit an exponential curve and a formula for dose fraction was developed. This model was later used to calculate gamma dose due to hot particle exposures by Durham in VARSKIN MOD2 (Durham and Lantz 1991).

Miller and Reece have also derived a model which can be used to calculate CPE corrected doses from hot particle exposures. First, an interaction point is selected and the angle through which secondary electrons must scatter in order to reach the dose point is calculated. Next, the probability of an electron scattering at the desired angle is calculated using the Klien-Nishina Formula. The charged particle slowing down approximation is then used to calculate the stopping power at the dose point. Finally, integration is performed over all dose points. Figure 4 illustrates the data obtained from this model (Miller and Reece 1990).

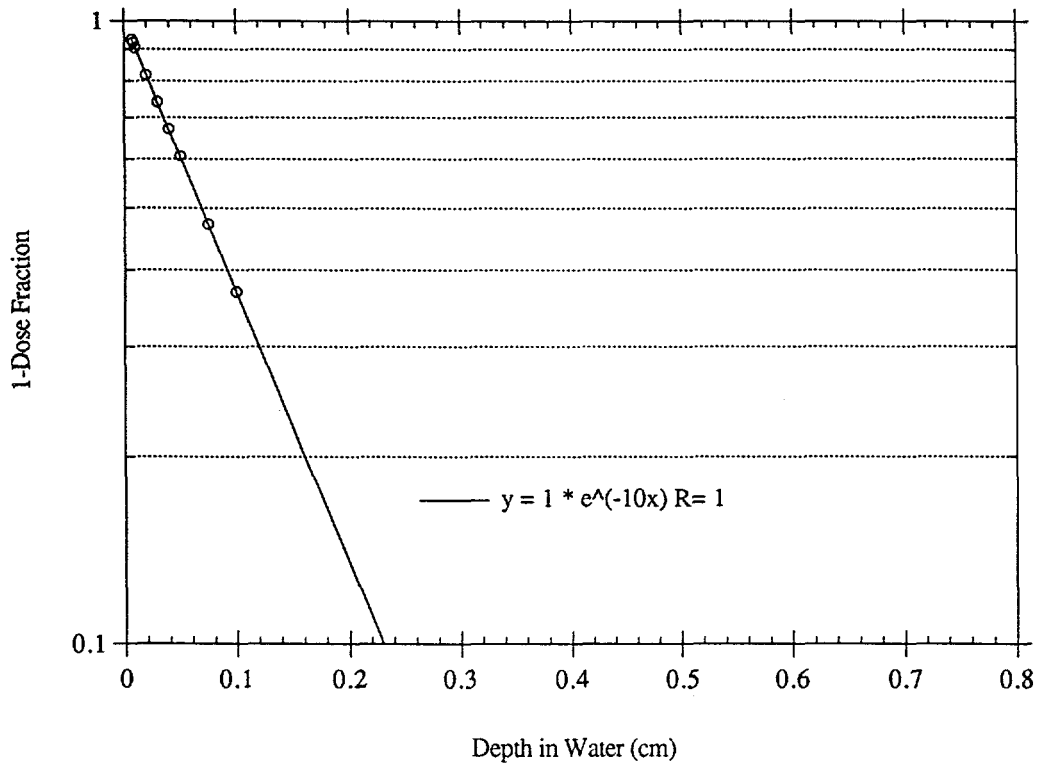

Fig. 3. Dose fraction as a function of depth in water for the Lantz-Lambert model.

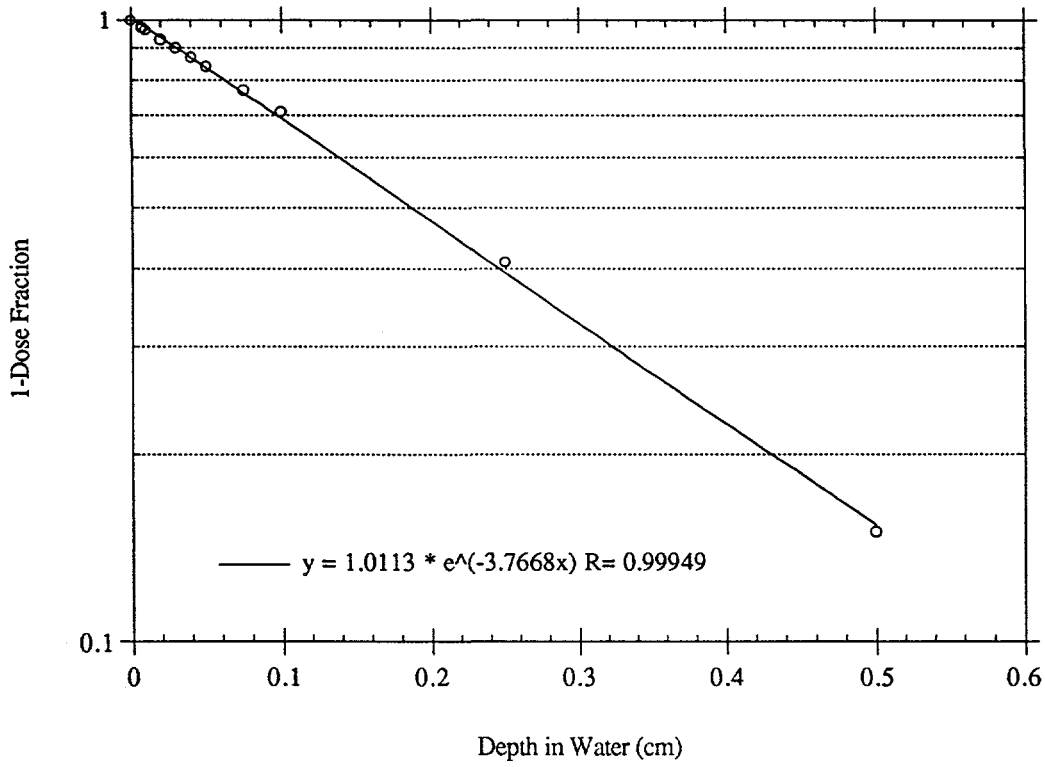

Fig. 4. Dose fraction as a function of depth in water for the Miller-Reece model.

Problem Summary

The CPE fractions and doses predicted by the Miller and Reece (1990) model vary significantly from those predicted by Chabot (1990), Durham (1992), Lantz, and Lambert (1990). The purpose of this research is to measure dose from ^{60}Co hot particle exposures as a function of depth using radiochromic dye film. These measurements will be compared to doses calculated using Equation (2), VARSKIN MOD2, and the Miller and Reece model.

Radiochromic Dye Film

The National Institute of Standards and Technology has used radiochromic dye films for high-dose gamma-ray dosimetry for several years. The addition of a laser scanning densitometer to counting systems makes these films useful in dose profiling (Soares et al. 1990). The low atomic number of the plastic film material makes it an ideal tissue equivalent dosimeter.

Radiochromic dosimeters are available in various forms such as thin films, thick films, gels, liquid solutions, and liquid-core waveguides. The radiochromic dye film used in this experiment, Gafchromic® film, consists of a thinly coated radiation sensitive layer (7 μm thick) on a 102 μm thick polyester substrate. The transparent film is colorless and almost grainless. Exposure to radiation causes the film to develop a deep blue color roughly proportional to dose. The film has a tissue equivalent response to electrons, gamma rays, and x-rays under charged particle equilibrium conditions (GAF Chemicals Corporation 1990).

The optical density or absorbance of Gafchromic® films is easily measured with photoelectric color densitometers, scanning densitometers, or spectrophotometers. The optical density of the irradiated film can be related to dose through the use of calibration curves (McLaughlin et al. 1994). The dose range of Gafchromic® film is 20 to 3000 Gy when read at the absorption peaks of 650 nm or 510 nm. The dose range of radiochromic films is dependent upon the manufacturing methods, this allows for the selection of film based upon the dose range of interest (GAF Chemicals Corporation 1990).

The primary problems with radiochromic dye films arise from the plastic in which the radiation sensitive dye is dissolved. The host material is responsible for most changes in radiation response due to varying temperature and humidity. The dose response of the film to radiation increases with temperature. A correction factor of 0.5% per °C up to 50 °C has been established for Gafchromic® film. Dose response decreases with increasing relative humidity at the rate of 0.25% per percent relative humidity (GAF Chemicals Corporation 1990). Accuracy of dose measurement is also affected by scratches on the film, uneven dye distribution, and uneven film thickness. All thin film dosimeters are affected slightly by ultraviolet light. Unlike those of most chemical and physical dosimeters, the responses of tissue equivalent radiochromic films are energy independent over a range of approximately 10 to 1250 keV when measuring doses in tissue or tissue equivalent materials (McLaughlin et al. 1984).

Radiochromic dye films are insensitive to light above 300 nm. Only a slight increase in color intensity will occur with time if the film is stored under controlled laboratory

conditions (Saylor et al. 1988). Film color develops fully after 24 hours post-irradiation. Film reading usually is delayed at least one day to avoid skewed results caused by post-irradiation darkening. In order to reduce undesirable effects, nonirradiated film should be stored in a dark area under constant temperature and humidity (GAF Chemicals Corporation 1990).

CHAPTER III

MATERIALS AND METHODS

Scanning Densitometer

A scanning system developed for use in previous research was modified for this experiment. The scanning system can be used to read the optical density of the radiochromic dye film in small increments along the X-Y plane. The scanning system consists of a light source, focusing system, photosensing detector, and precision computer controlled linear translation tables. A light emitting diode (LED) is the light source for the system. The proportion of light transmitted through the film is measured photometrically. System components include: a photomultiplier tube (PMT), single channel analyzer (SCA), amplifier, linear translation tables actuated with stepping motors, IBM compatible computer, 200 μm pinhole, LED, and two condensing lenses and a double concave lens to gather and focus the light. A design scheme of the scanning system is shown in Fig. 5.

The maximum absorption wavelength of the film is near 630 nm. The LED was chosen as the light source because it emits light in the 600-680 nm band. This wavelength closely matches the absorption peak of the film. The amount of light transmitted through the film is measured by the PMT. The transmitted light intensity is converted to electrical pulses in the PMT. The SCA receives the pulses from the PMT and converts them to counts.

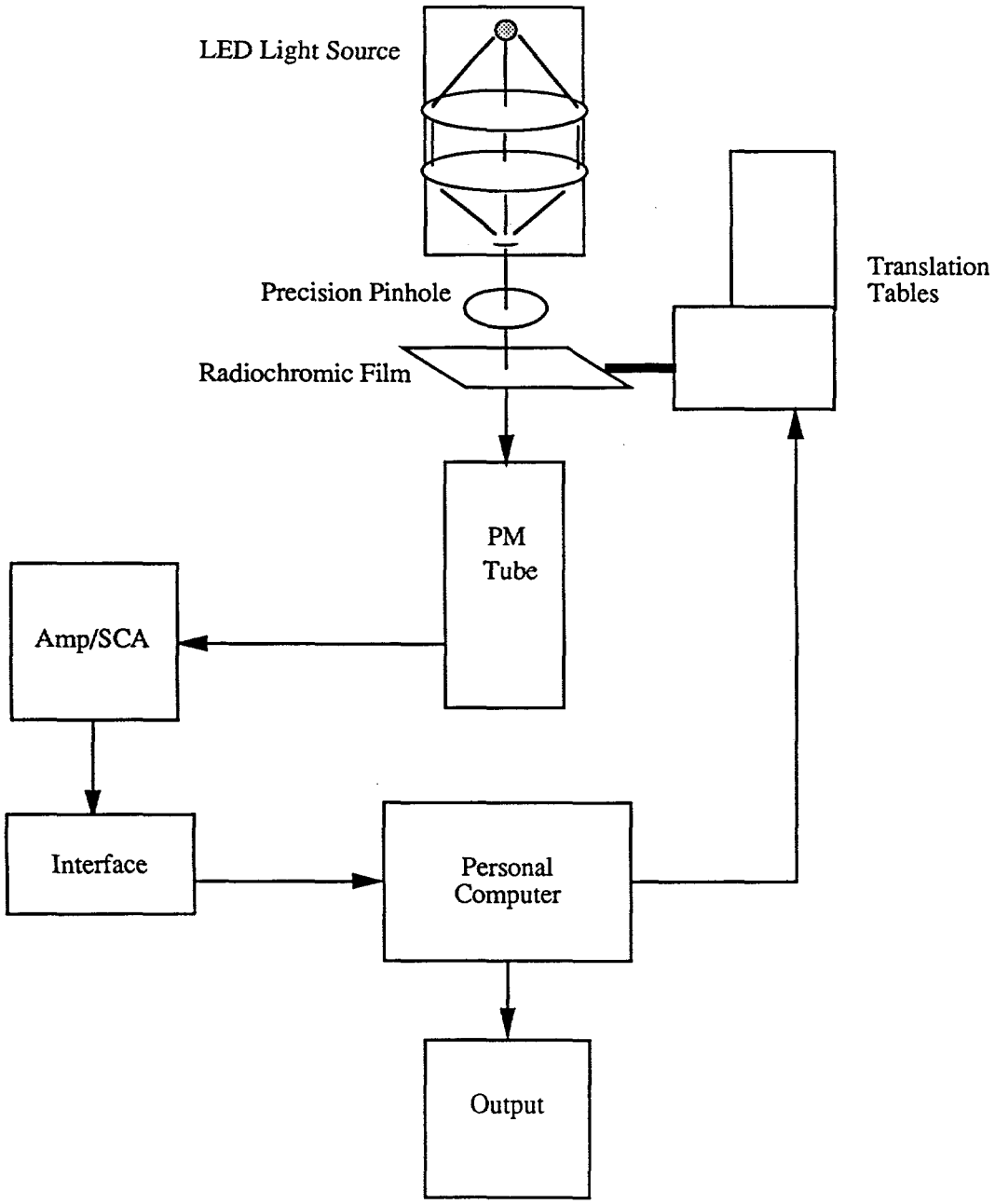

Fig. 5. Design scheme of scanning densitometer.

Initially, the light source was too intense to be directed into the PMT. Even at low voltages the PMT was completely saturated. A process of trial and error was used to find the optimal light intensity and operating voltage. The LED beam was set at the focal length of one condensing lens and the resulting beam refocused by a second condensing lens. This focused light was recollimated into a narrow beam by a double concave lens.

A flat metal table served as the base for the entire scanning system. A 200 μm precision pinhole was mounted approximately 25.4 mm above the table and directly over a 3.18 mm diameter hole in the base table. The LED and lenses were encased in a metal tube and attached to an arm above the pinhole.

A PMT encased in a light-tight container was fixed beneath the 3.18 mm hole in the table. Light transmitted through the film is detected by the PMT. Fine adjustment was required to maximize the SCA count rate and the amount of light reaching the PMT. Upon completion of these adjustments, films were scanned by interposing them between the pinhole and the table base.

Two precision linear translation tables were mounted to the base table at ninety degree angles to each other. The tables were originally manual translation tables, but were modified by mounting stepping motors to each table to allow movement under computer control. An arm, interposed between the pinhole and the hole in the base table was attached to the linear translation tables, held the film and moved with the translation tables.

A groove cut in the arm allowed for the placement of a film holder. To facilitate film placement, the film holder was designed to be removed from the scanning system. Once the film was secured in the holder it was placed into the arm of the translation table.

The film holder consisted of a flat metal piece with an oval cut into it to allow light to pass through the film. A second, slightly smaller, metal piece with an oval cut into it was used to secure the film in the holder. The two pieces of metal fit tightly together and prevented unwanted movement of the film during scanning. The entire scanning system was placed in a sealed box to prevent exposure to light.

The translation tables with stepping motors were controlled using a BASIC computer code. The computer program allowed the tables to be adjusted in the X-and Y-direction from the computer keyboard. The tables could also be programmed to move over a matrix of any size at any step interval. An area would be scanned automatically after the overall X and Y distance to be traveled and the step interval were input into the program.

After the translation tables moved the film to the first location to be scanned, the counts from the SCA were recorded by the computer. SCA count time is determined by the user, and input into the computer prior to scanning. A count time of 10 seconds was long enough to acquire a statistically valid number of counts, but short enough to scan the films in a reasonable amount of time.

Prior to beginning a scan, all input variables were loaded and the film was positioned at the first point to be scanned. The computer would record the counts registered by the SCA at the end of the count time, the Y-axis translation table would then move the film the preset step size and the SCA would once again begin its count and record the data at the end of the counting period. This process would continue until the specified Y-axis distance was traveled. At the end of the Y-axis, the tables would move the film one step along the X-axis and follow the Y-axis all the way back to the 0 point, and then move another step

along the X-axis. This continued until all points on both the X and Y-axis were scanned. The collected data was stored in the following form: X distance, Y distance, step size, count time, and counts at each point.

A FORTRAN program was used to convert counts to optical density and then to absorbed dose. This program required the user to input the background count rate and the calibration equation at the time of the scan. The data file produced by the scan was also read. Optical density (OD) was calculated using the following equation (Attix 1986):

$$OD = \log \frac{I_o}{I} \tag{18}$$

where, I_0 = the amount of light incident on the film,

and I = the amount of light transmitted through the film.

After the SCA counts were converted to optical density, the FORTRAN program used the calibration equation to calculate the absorbed dose rates at each point along the film. The FORTRAN program output was arranged in the same matrix form as it was scanned. Dose rates were reported in Gy/h.

Film Calibration

To relate dose to optical density, a series of films were exposed to the ^{60}Co source at the Zachry Engineering Center. The Radiation Safety Office (RSO) at TAMU determined the source to have a dose rate of 1.22 Gy/min at a distance of 0.3 m from the source. Exposure times for the calibration films ranged from 40 minutes to 7 hours, resulting in doses ranging from 50 to 500 Gy delivered to the films.

The films were placed in photographic film holders in order to prevent exposure to light. Fifty-to-seventy five millimeter long pieces of film were taped to the film holder. The photographic film holder was placed one foot from the source with the sensitive side of the film facing the beam. A 1 cm plexiglass plate was placed in front of the film holder to ensure that charged particle equilibrium was established. The exposures were performed over a one week period and the films were allowed to stabilize at least one day prior to reading.

Radiochromic dye film is sensitive to handling, easy to scratch, and easy to mar with fingerprints on the surface. Due to the sensitivity of film, three calibration sets were made as a precautionary measure and to insure reproducibility among films. Three film strips were placed in the photographic film holder and irradiated simultaneously. The calibration films compared closely to calibrations performed for previous research (Shaw 1993). Differences between calibrations performed for previous research and the current calibration curves can be attributed to changes made in the scanning densitometer. For example, the light source was changed from a HeNe laser to a LED, lenses were used to focus the light instead of a prism, the PMT was replaced, and the operating voltage of the PMT was increased from 975 V to 1050 V.

After irradiation, the films were removed from the photographic film holders and were taped to standard size sheets of paper marked with the dose and irradiation time. The paper was folded in half to prevent scratching of the film. In order to prevent abrasions, the films were handled by pieces of tape affixed to each end. All of the calibration films were kept in descriptive sheets which were placed in a manila folder. In addition, a piece of

unexposed film was used as a control. The unexposed film was labeled and scanned in the same manner as the other calibration films. This unexposed piece of film served as the 0 Gy exposure.

Each film was placed in the scanning system and five 10-second counts were recorded. These counts were averaged and the optical density calculated. A calibration curve was constructed by plotting the average optical density versus dose delivered to each film. A third-order polynomial equation fit the calibration curve. Figure 6 illustrates a typical calibration curve.

Hot Particle Preparation

The hot particle was placed in a source holder prior to film exposure. The holder consisted of a flat outer ring and a pipelike inner ring. A schematic of the hot particle holder and film exposure methodology is shown in Fig. 7. A sheet of mylar measuring 70 μm thick was secured over the inner ring. The outer ring was then snapped onto the inner ring to help hold the mylar in place. The holder did not have a backing plate, as it was designed to imitate actual hot particle exposures as closely as possible. The presence of a backing plate would cause backscatter which does not occur in real hot particle exposures. Backscatter from the holder itself was negligible due to the diameter of the inner ring.

The hot particle was picked up with a piece of scotch tape and then placed in the center of the mylar, thus securing the hot particle between the mylar and the tape. The

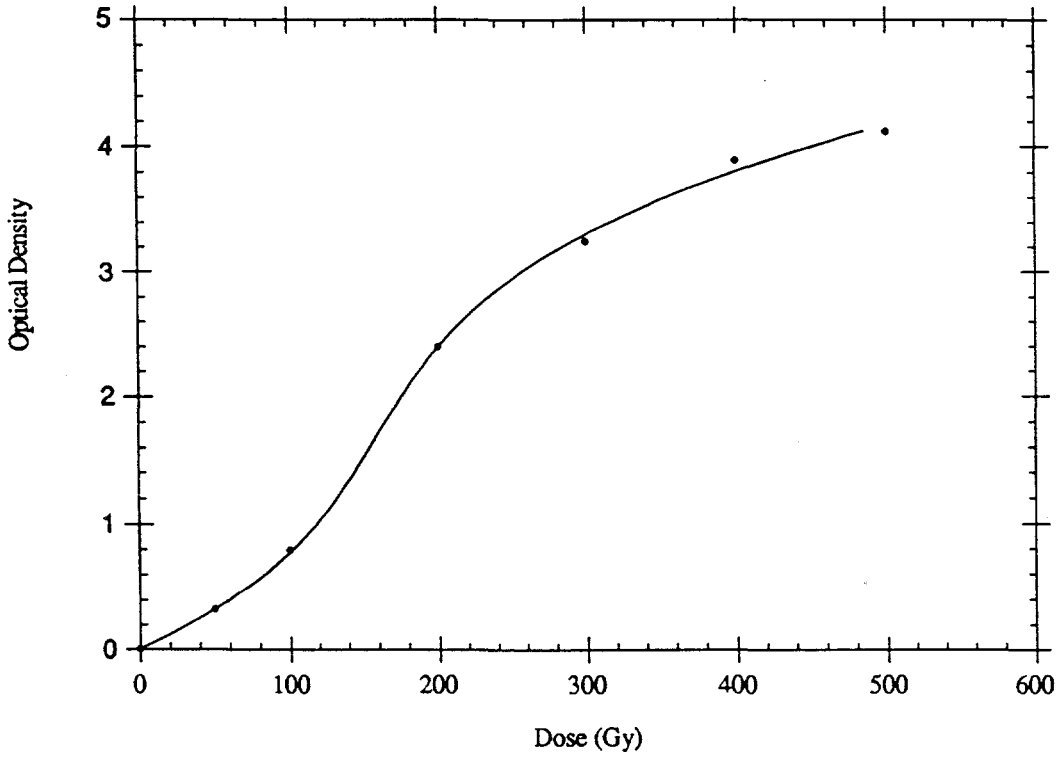

Fig. 6. Typical calibration curve for scanning densitometer and radiochromic dye film.

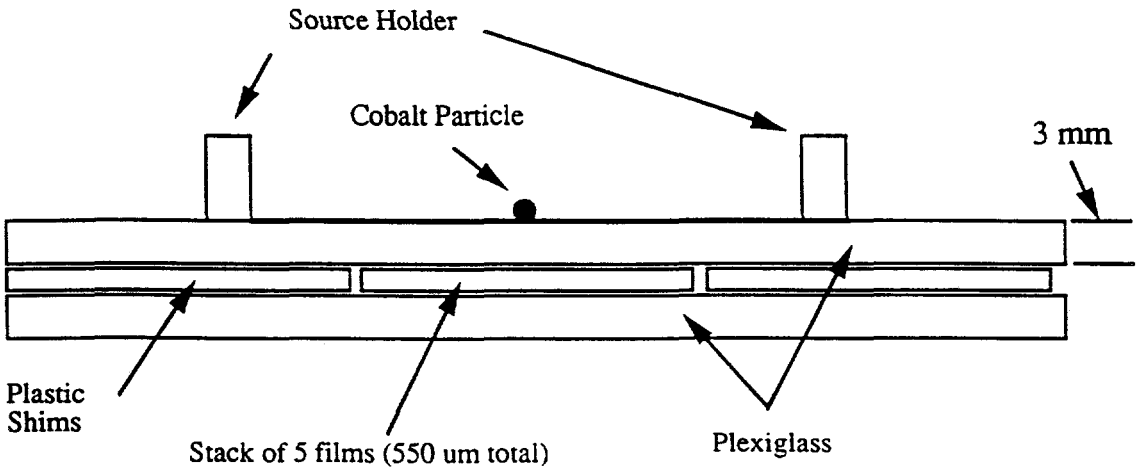

Fig. 7. Schematic of hot particle holder and film exposure methodology.

mylar side of the source holder was placed face down onto the film to be irradiated. This design interposed the thin sheet of mylar between the hot particle and the irradiation site. The hot particle was left in the same configuration throughout the experiment.

Film Exposures

Stacks of radiochromic dye film were exposed to determine the dose versus depth profiles of the hot particle. The films were scanned using the densitometer and the lateral doses as a function of depth were measured. The stack of five films was used to measure depth-dose profiles. The stacking of films allowed the experimenter to obtain several depth-dose profiles in a single measurement rather than a measurement at each depth. Shallow dose measurements were completed with the hot particle in contact with a thin tissue equivalent layer placed over the plastic film. A 3.18 mm piece of plexiglass was interspersed between the film and the hot particle in order to obtain deep dose measurements. The films were exposed for times varying from 400 minutes to 23 hours and are listed in Table 1.

The films for the hot particle exposures were handled in the same way as the calibration films. Approximately 35 to 50 mm of film was exposed to the hot particle. The film was handled with tape placed on each end and was placed in a folded identification sheet containing a description of the exposure.

Prior to exposure, the films were stacked and taped to a plexiglass board. The plexiglass supplied backscatter as would an individual's body during an actual exposure. The films were surrounded by tissue equivalent material in order to maintain a uniform

Table 1. Film exposures performed.

Exposure	Exposure Time (h)	Depth (mm)
1	3.33	0.235
	3.33	0.345
	3.33	0.455
	3.33	0.565
	3.33	0.675
2	10	0.235
	10	0.345
	10	0.455
	10	0.565
	10	0.675
3	23	2.51
	23	2.62
	23	2.73
	23	2.84
	23	2.95

scattering environment around the film and a thin sheet of tissue equivalent material was placed over the film. Care was taken to ensure the sensitive side of the film faced upward toward the hot particle. The hot particle was positioned through the use of an outline on the top layer of tissue equivalent material. Some of the exposures completed were not useful as the film was saturated or underexposed. However, once the hot particle was removed from the film it could not be replaced because it would be impossible to return it to its original location.

Film Scanning and Processing

A scan of the set of calibration films was completed each day before film scanning was begun. The films were loaded into the densitometer in the dark in order to prevent light excitation of the PMT. Room lights were utilized after the lid of the box containing the densitometer was closed. The area of the film exposed was difficult to position in the scanning system because it varied from film to film. For this reason, a coarse scan was performed to determine the area of interest on the film. After evaluation of the coarse scan, the translation tables were repositioned to scan the film area of interest with a small step size.

The calibration curve was used to convert the data obtained from the scans to dose at each position scanned. The third order polynomial equation from the day's calibration was input into a FORTRAN program which was used to convert optical density to dose. The calibrations and film scans were labeled by the date they were performed. In order to prevent small day to day variations in the scanning system and calibrations, the calibration

equation used in the FORTRAN program was taken from a calibration performed the day the film was scanned. The absorbed dose rate output was imported into graphics program for further analysis. The data was in matrix form, the location in the matrix corresponded to the physical position on the film. The X-axis position was read from left to right and the Y-axis positions ran from top to bottom. This format allowed the dose rate at any point on the film to be determined. The position of the center of the source on the film was located by identifying the area of maximum dose rates and following the X and Y axis out from the center point. The dose values surrounding the center point were then checked for symmetry to assure that a spurious high dose point was not chosen.

CHAPTER IV

RESULTS AND DISCUSSION

Deep Exposures

The deep exposure data discussed in this section is typical of the data obtained. The term deep exposure refers to measurements at vertical depths ranging from 2.51 mm to 2.95 mm. To measure deep exposure, films were exposed to the hot particle source for a period of 23 h. As described earlier, the data matrix for the 2.73 mm depth exposure was evaluated to find the center of the hot particle. As expected, the data points gradually increased as they approached the centerline and then began a steady decrease. The error in the measured dose rates does not exceed 8%. Figure 8 is a plot of dose rate 2.73 mm below the source as a function of horizontal distance from the center of the hot particle. The center of the hot particle is not necessarily located at zero.

As shown earlier, eqn (2) defines dose with respect to the specific gamma ray constant.

$$D = \frac{\Gamma A_o}{r^2}$$

As a check, dose multiplied by the distance squared can be plotted against total distance.

$$D \cdot r^2 = A_o \Gamma = k \qquad (19)$$

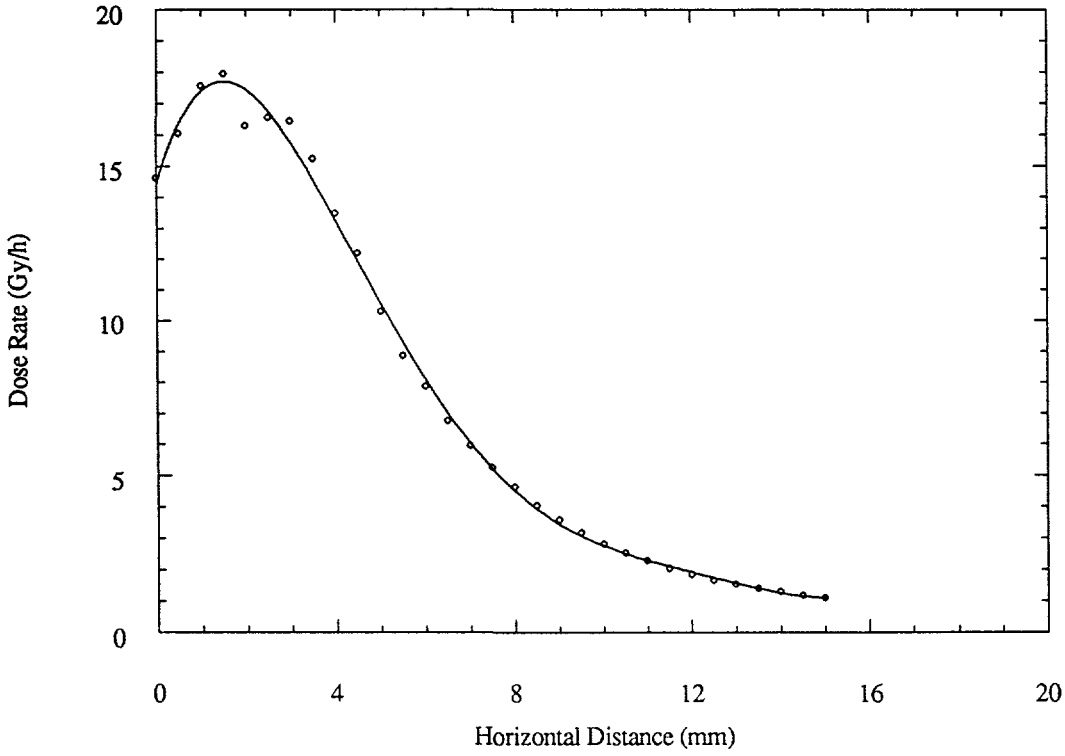

Fig. 8. Dose rate 2.73 mm below source as a function of horizontal distance.

This experimental gamma constant was calculated for each data point by multiplying the dose rate by the square of the distance traveled by the gamma ray through the plastic to reach the dose point. The distance traveled through the plastic was found by solving for the hypotenuse of the right triangle formed by the vertical depth of the film and the horizontal distance of the dose point on the film. Figure 9 is a diagram of the right triangle formed by the depth and distance of the dose point from the source.

The specific gamma ray constant can only be used when photons travel through a nonattenuating media. The law of exponential attenuation can be applied to determine the effect of the plastic:

$$\frac{I}{I_o} = e^{-\frac{\mu}{\rho}t} \qquad (20)$$

where, I is the attenuated fluence, I_0 is the initial fluence, $\frac{\mu}{\rho}$ is the mass attenuation coefficient, and t is the thickness of the media. The $\frac{\mu}{\rho}$ value for 1.250 MeV gamma rays in plexiglass is 0.06225 ($cm^2\ g^{-1}$), ρ is 1.19 ($g\ cm^{-3}$) and t is 20 mm (Attix 1986). The fluence is attenuated 14% by 20 mm of plexiglass tissue equivalent material.

Figure 10 is a plot of the experimental gamma constant as a function of distance traveled through plexiglass. The data used to create Fig. 10 are given in Table 2. The experimental gamma constant is the specific gamma constant multiplied by the source strength which is found to be 555 MBq. As the distance traveled by the gamma ray increases, the experimental gamma constant approaches a single value because the secondary electrons produced by the gamma rays come into equilibrium with the photons.

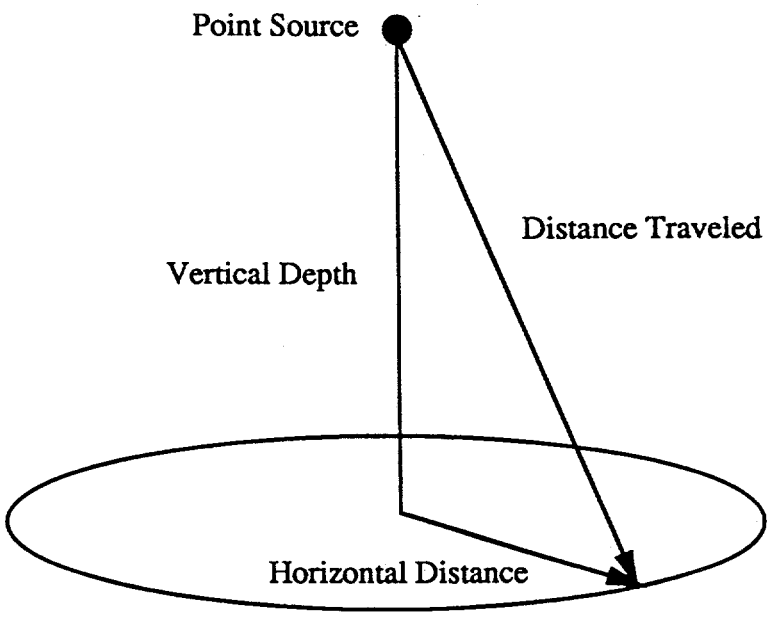

Figure 9. Right triangle formed by depth and distance from point source.

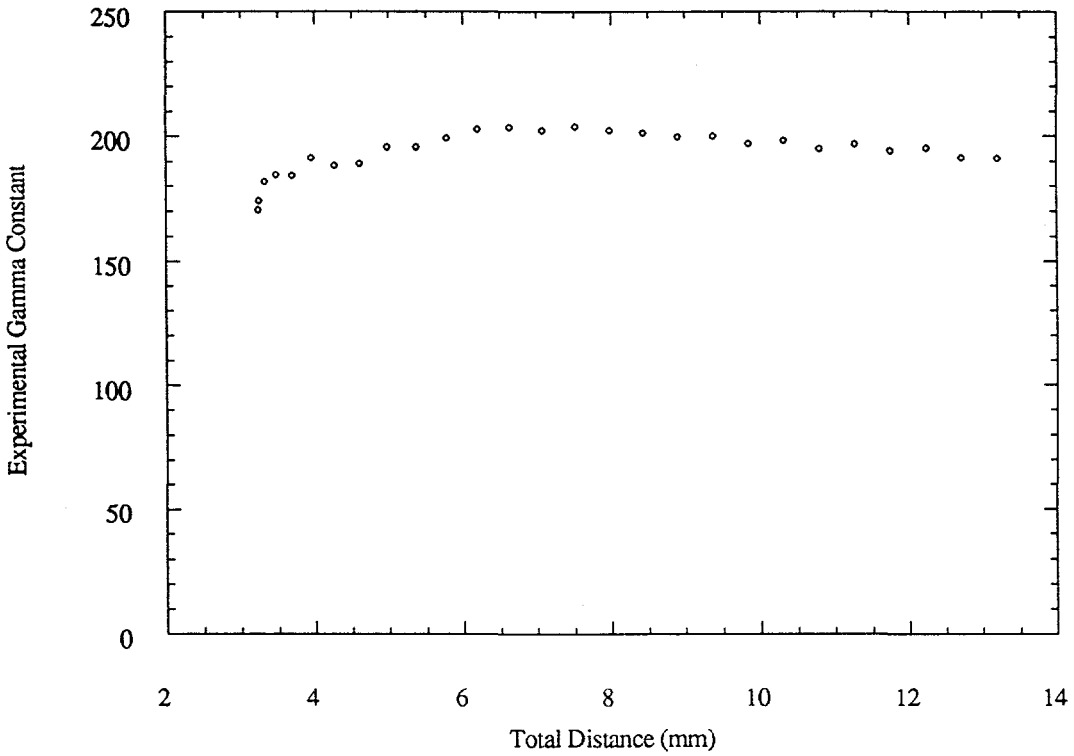

Fig. 10. Experimental gamma constant as a function of distance traveled in tissue equivalent plastic for the 2.73 mm deep exposure.

Table 2. Data obtained from the exposure at a depth of 2.73 mm.

Horizontal Distance (mm)	Dose Rate (Gy/h)	Distance Squared	Distance (mm)	Experimental Gamma Constant
0.0000	14.618	15.263	3.9067	223.11
0.50000	16.052	13.313	3.6486	213.69
1.0000	17.546	11.863	3.4442	208.14
1.5000	17.953	10.913	3.3034	195.92
2.0000	16.297	10.463	3.2346	170.51
2.5000	16.565	10.513	3.2423	174.14
3.0000	16.428	11.063	3.3260	181.73
3.5000	15.240	12.113	3.4803	184.60
4.0000	13.483	13.663	3.6963	184.21
4.5000	12.186	15.713	3.9639	191.47
5.0000	10.310	18.263	4.2735	188.29
5.5000	8.8700	21.313	4.6166	189.04
6.0000	7.8704	24.863	4.9862	195.68
6.5000	6.7709	28.913	5.3770	195.76
7.0000	5.9557	33.463	5.7847	199.29
7.5000	5.2665	38.513	6.2058	202.83
8.0000	4.6226	44.063	6.6380	203.68
8.5000	4.0396	50.113	7.0790	202.43
9.0000	3.5983	56.663	7.5275	203.89
9.5000	3.1752	63.713	7.9820	202.30
10.000	2.8243	71.263	8.4417	201.27
10.500	2.5204	79.313	8.9058	199.90
11.000	2.2765	87.863	9.3735	200.02
11.500	2.0335	96.913	9.8444	197.07
12.000	1.8617	106.46	10.318	198.21
12.500	1.6730	116.51	10.794	194.93
13.000	1.5483	127.06	11.272	196.73
13.500	1.4057	138.11	11.752	194.14
14.000	1.3043	149.66	12.234	195.21
14.500	1.1830	161.71	12.717	191.31
15.000	1.0970	174.26	13.201	191.16

The experimental gamma constant for this plot was approximately 200. The other exposures, as expected, also have experimental gamma constants in the range of 200. The experimental gamma constant was expected to have the same value under CPE conditions for all exposures because gamma constants are radionuclide specific and the films were all exposed to the same radionuclide.

Shallow Exposures

The shallow exposure data discussed in this section is typical of the data obtained. The phrase "shallow exposures" refers to films at vertical depths ranging from 0.235 to 0.675 mm below the hot particle source. As shown earlier in Table 1, shallow exposures were performed for periods of 3.33 h and 10 h. These shallow exposures allowed a comparison of doses delivered at the same depths but with different exposure times and ensured the reproducibility of the data. Figures 11 and 12 are plots of the dose rate 0.235 mm below the source as a function of horizontal distance. These figures were created in the same manner as those for the deep exposures. The data used in Figs. 11 and 12 are listed in Tables 3 and 4. The dose delivered to the area below the center of the hot particle saturated the radiochromic dye film. This caused fluctuations and inconsistencies in dose rates between the two plots as can be seen in Figs. 11 and 12. To correct this, all dose points greater than 400 Gy were removed from the data. Tables 5 and 6 list the modified data. Figure 13 is a comparison of dose rate as a function of distance for the 10 h and 3.33 h exposure periods. As expected, the modified plots yield the same dose rate at a given depth even though the time of exposure is different. Dose rates at a given depth but

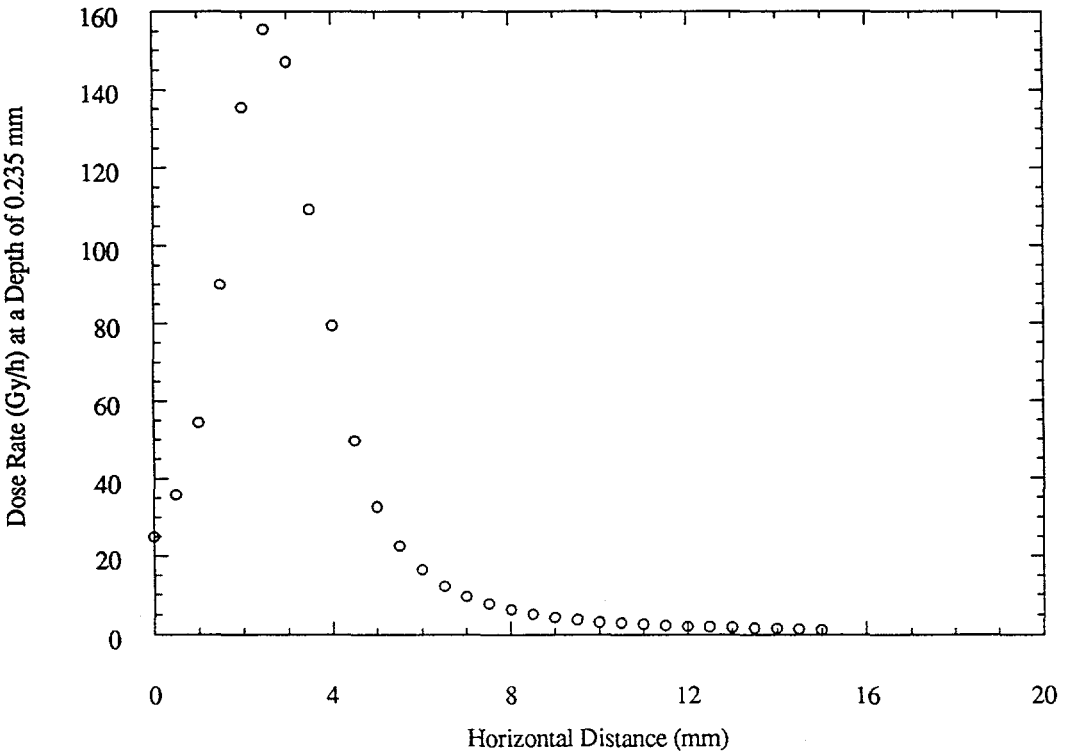

Fig. 11. Dose rate as a function of distance for the 3.33 h exposure.

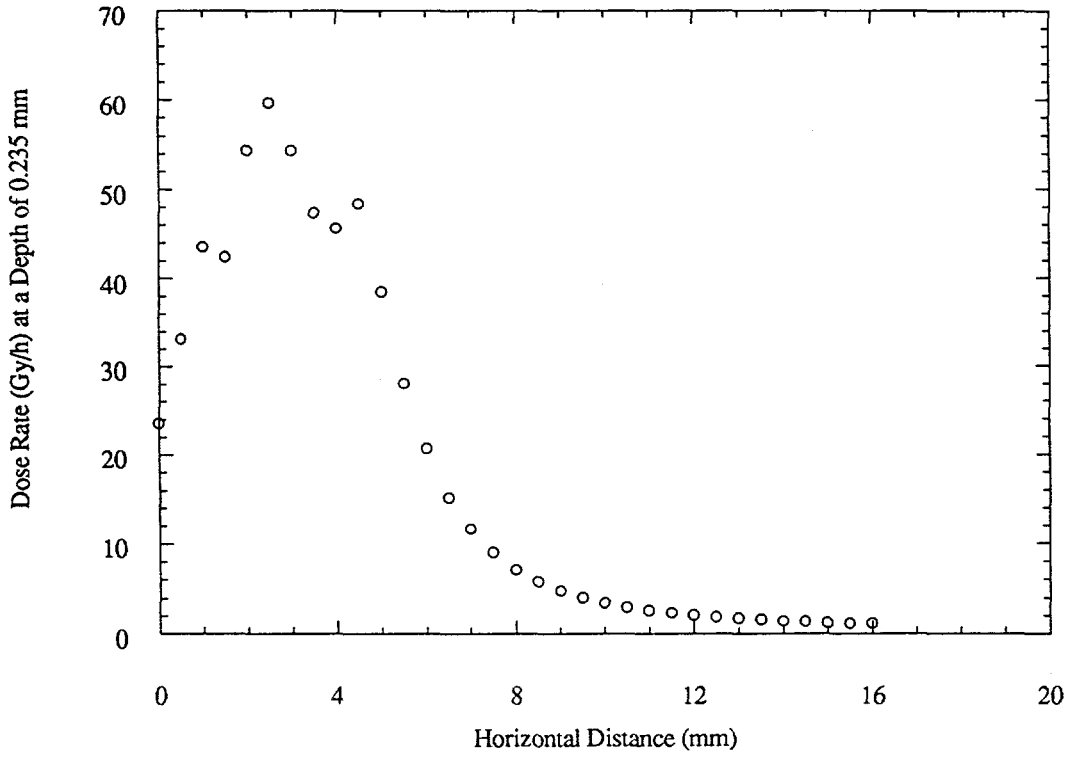

Fig. 12. Dose rate as a function of distance for the 10 h exposure.

Table 3. Data from 0.235 mm depth for a 3.33 h exposure period.

Horizontal Distance (mm)	Dose Rate (Gy/h)	Distance Squared	Distance (mm)	Experimental Gamma Constant
0.0000	24.853	6.0629	2.4623	150.68
0.5000	35.805	3.9629	1.9907	141.89
1.0000	54.399	2.3629	1.5372	128.54
1.5000	89.949	1.2629	1.1238	113.59
2.0000	135.27	0.6628	0.8141	89.669
2.5000	155.43	0.5628	0.7502	87.487
3.0000	147.01	0.9628	0.9812	141.55
3.5000	109.31	1.8629	1.3649	203.62
4.0000	79.502	3.2629	1.8063	259.40
4.5000	49.649	5.1629	2.2722	256.33
5.0000	32.640	7.5629	2.7501	246.85
5.5000	22.550	10.463	3.2346	235.93
6.0000	16.450	13.863	3.7233	228.05
6.5000	12.162	17.763	4.2146	216.03
7.0000	9.5495	22.163	4.7077	211.65
7.5000	7.7207	27.063	5.2022	208.94
8.0000	6.2432	32.463	5.6976	202.67
8.5000	5.1231	38.363	6.1938	196.54
9.0000	4.3363	44.763	6.6905	194.11
9.5000	3.7778	51.663	7.1877	195.17
10.000	3.1381	59.063	7.6852	185.35
10.500	2.8619	66.963	8.1831	191.64
11.000	2.6066	75.363	8.6812	196.44
11.500	2.2583	84.263	9.1795	190.29
12.000	2.0360	93.663	9.6780	190.70
12.500	1.9820	103.56	10.177	205.26
13.000	1.7568	113.96	10.675	200.21
13.500	1.6847	124.86	11.174	210.35
14.000	1.5616	136.26	11.673	212.78
14.500	1.3874	148.16	12.172	205.56
15.000	1.1802	160.56	12.671	189.49

Table 4. Data from 0.235 mm depth for a 10 h exposure period.

Horizontal Distance (mm)	Dose Rate (Gy/h)	Distance Squared	Distance (mm)	Experimental Gamma Constant
0.0000	23.614	5.8304	2.4146	137.68
0.5000	33.147	3.7804	1.9443	125.31
1.0000	43.570	2.2304	1.4934	97.177
1.5000	42.446	1.1804	1.0864	50.102
2.0000	54.369	0.6303	0.7939	34.273
2.5000	59.655	0.5803	0.7618	34.622
3.0000	54.369	1.0304	1.0151	56.020
3.5000	47.382	1.9804	1.4073	93.834
4.0000	45.636	3.4304	1.8521	156.55
4.5000	48.411	5.3804	2.3196	260.47
5.0000	38.532	7.8304	2.7983	301.72
5.5000	28.106	10.780	3.2833	302.99
6.0000	20.759	14.230	3.7723	295.41
6.5000	15.241	18.180	4.2638	277.09
7.0000	11.718	22.630	4.7571	265.18
7.5000	9.1080	27.580	5.2517	251.20
8.0000	7.1380	33.030	5.7472	235.77
8.5000	5.7950	38.980	6.2434	225.89
9.0000	4.7810	45.430	6.7402	217.20
9.5000	4.0430	52.380	7.2374	211.77
10.000	3.4710	59.830	7.7350	207.67
10.500	2.9970	67.780	8.2329	203.14
11.000	2.6190	76.230	8.7310	199.65
11.500	2.3570	85.180	9.2293	200.77
12.000	2.0880	94.630	9.7278	197.59
12.500	1.8810	104.58	10.226	196.72
13.000	1.7540	115.03	10.725	201.76
13.500	1.5920	125.98	11.224	200.56
14.000	1.4290	137.43	11.723	196.39
14.500	1.3970	149.38	12.222	208.68
15.000	1.2730	161.83	12.721	206.01
15.500	1.1560	174.78	13.220	202.05
16.000	1.1500	188.23	13.720	216.46

Table 5. Modified data from 0.235 mm depth for a 3.33 h exposure period.

Horizontal Distance (mm)	Dose Rate (Gy/h)	Distance Squared	Distance (mm)	Experimental Gamma Constant
0.0000	24.853	6.0629	2.4623	150.68
0.5000	35.805	3.9629	1.9907	141.89
1.0000	54.399	2.3629	1.5372	128.54
1.5000	89.949	1.2629	1.1238	113.59
3.5000	109.31	1.8629	1.3649	203.62
4.0000	79.502	3.2629	1.8063	259.40
4.5000	49.649	5.1629	2.2722	256.33
5.0000	32.640	7.5629	2.7501	246.85
5.5000	22.550	10.463	3.2346	235.93
6.0000	16.450	13.863	3.7233	228.05
6.5000	12.162	17.763	4.2146	216.03
7.0000	9.5495	22.163	4.7077	211.65
7.5000	7.7207	27.063	5.2022	208.94
8.0000	6.2432	32.463	5.6976	202.67
8.5000	5.1231	38.363	6.1938	196.54
9.0000	4.3363	44.763	6.6905	194.11
9.5000	3.7778	51.663	7.1877	195.17
10.000	3.1381	59.063	7.6852	185.35
10.500	2.8619	66.963	8.1831	191.64
11.000	2.6066	75.363	8.6812	196.44
11.500	2.2583	84.263	9.1795	190.29
12.000	2.0360	93.663	9.6780	190.70
12.500	1.9820	103.56	10.177	205.26
13.000	1.7568	113.96	10.675	200.21
13.500	1.6847	124.86	11.174	210.35
14.000	1.5616	136.26	11.673	212.78
14.500	1.3874	148.16	12.172	205.56
15.000	1.1802	160.56	12.671	189.49

Table 6. Modified data from 0.235 mm depth for a 10 h exposure period.

Horizontal Distance (mm)	Dose Rate (Gy/h)	Distance Squared	Distance (mm)	Experimental Gamma Constant
0.0000	23.614	5.8304	2.4146	137.68
0.5000	33.147	3.7804	1.9443	125.31
5.0000	38.532	7.8304	2.7983	301.72
5.5000	28.106	10.780	3.2833	302.99
6.0000	20.759	14.230	3.7723	295.41
6.5000	15.241	18.180	4.2638	277.09
7.0000	11.718	22.630	4.7571	265.18
7.5000	9.1080	27.580	5.2517	251.20
8.0000	7.1380	33.030	5.7472	235.77
8.5000	5.7950	38.980	6.2434	225.89
9.0000	4.7810	45.430	6.7402	217.20
9.5000	4.0430	52.380	7.2374	211.77
10.000	3.4710	59.830	7.7350	207.67
10.500	2.9970	67.780	8.2329	203.14
11.000	2.6190	76.230	8.7310	199.65
11.500	2.3570	85.180	9.2293	200.77
12.000	2.0880	94.630	9.7278	197.59
12.500	1.8810	104.58	10.226	196.72
13.000	1.7540	115.03	10.725	201.76
13.500	1.5920	125.98	11.224	200.56
14.000	1.4290	137.43	11.723	196.39
14.500	1.3970	149.38	12.222	208.68
15.000	1.2730	161.83	12.721	206.01
15.500	1.1560	174.78	13.220	202.05
16.000	1.1500	188.23	13.720	216.46

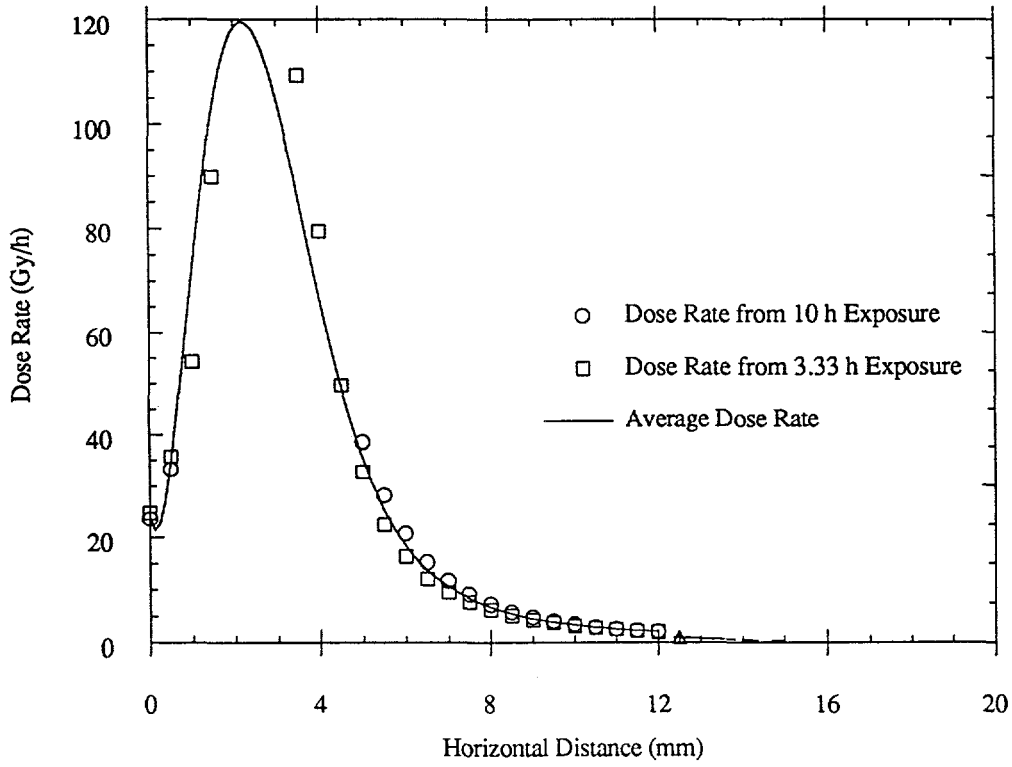

Fig. 13. A comparison of dose rate as a function of distance for the 10 h and 3.33 h exposure periods.

different exposure time are the same because the degree of CPE reached at the specified depth is the same regardless of the length of exposure to the source. This agreement between the dose rates lends some confidence that the data are reproducible. The error in the measured dose rates was found to be less than 8%.

Figures 14 and 15 are plots of the experimental gamma constant as a function of distance in tissue for the 3.33 h and 10 h exposures at a depth of 0.235 mm. The experimental gamma constant was calculated in the same manner as for deep exposures. The point source model failed at distances less than the radius of the hot particle. Due to the finite size of the hot particle, doses to the film area below the source increased instead of decreasing as a function of r^{-2}. Thus, the experimental gamma constant increased with the dose and then approached a single value when CPE was reached. The value of the experimental gamma constant for both exposures is 200 as was stated previously. Tables 5 and 6 illustrate the data utilized to create these figures.

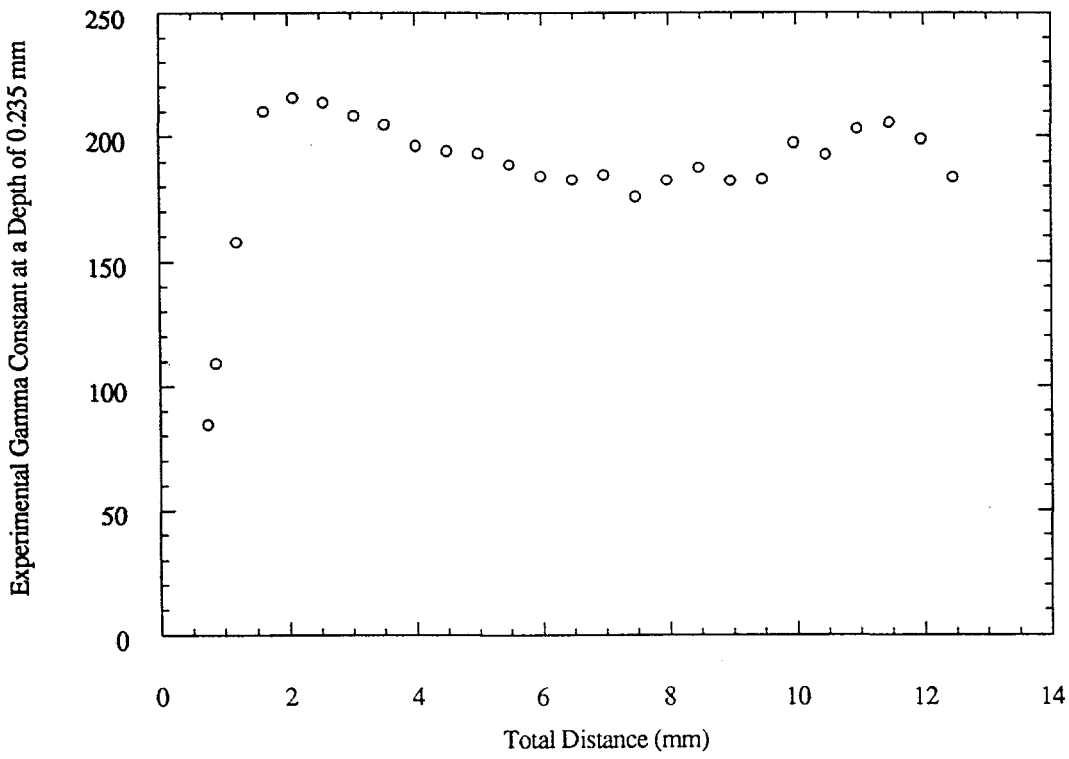

Fig. 14. Experimental gamma constant as a function of distance traveled in tissue equivalent plastic for the 3.33 h exposure.

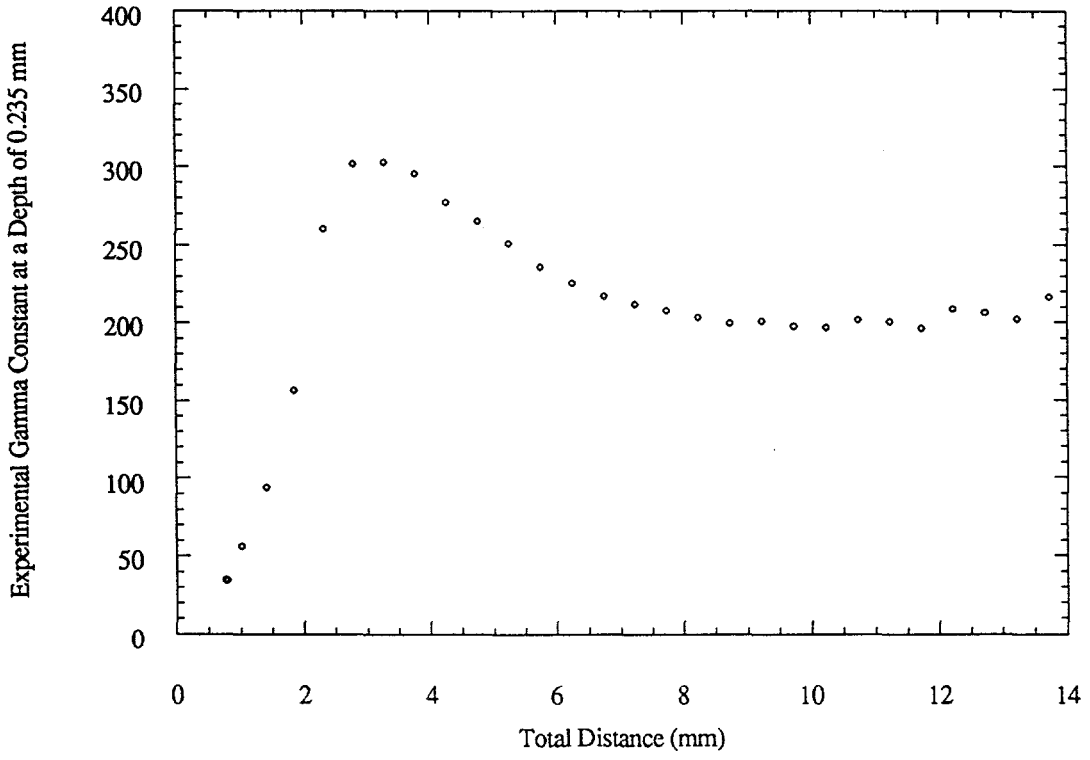

Fig. 15. Experimental gamma constant as a function of distance traveled in tissue equivalent plastic for the 10 h exposure.

CHAPTER V

CONCLUSIONS

Measurements have been made of charged particle equilibrium as a function of distance from a radiation source. The methodology used to measure beta doses from point source exposures (Shaw 1993) was used in this experiment and this methodology was found to be equally effective for determining gamma doses from point source exposures.

Radiochromic dye film was used to measure the ^{60}Co depth-dose profiles. The useful range of the radiochromic dye film for the experimental setup was determined to be 50-400 Gy. The scanning system was only capable of distinguishing doses between 20 and 400 Gy. The film was used to measure both shallow and deep doses.

Comparisons of the depth dose profiles for different exposure periods showed the data to be reproducible. The error in the calculated dose rates did not exceed 8%. An experimental gamma constant was calculated for all exposures and was found to be 200 regardless of the exposure period or depth.

The experimental dose rate measurements were compared to the Miller-Reece and Lantz-Lambert models. Comparisons of the experimental dose rates and the dose rates calculated by the Miller-Reece and Lantz-Lambert models are plotted in Figures 16, 17,18 and 19. The experimental data supports the Miller-Reece model. The expanded views of the comparisons between the measured and modeled dose rates (Figs. 17 and 19)

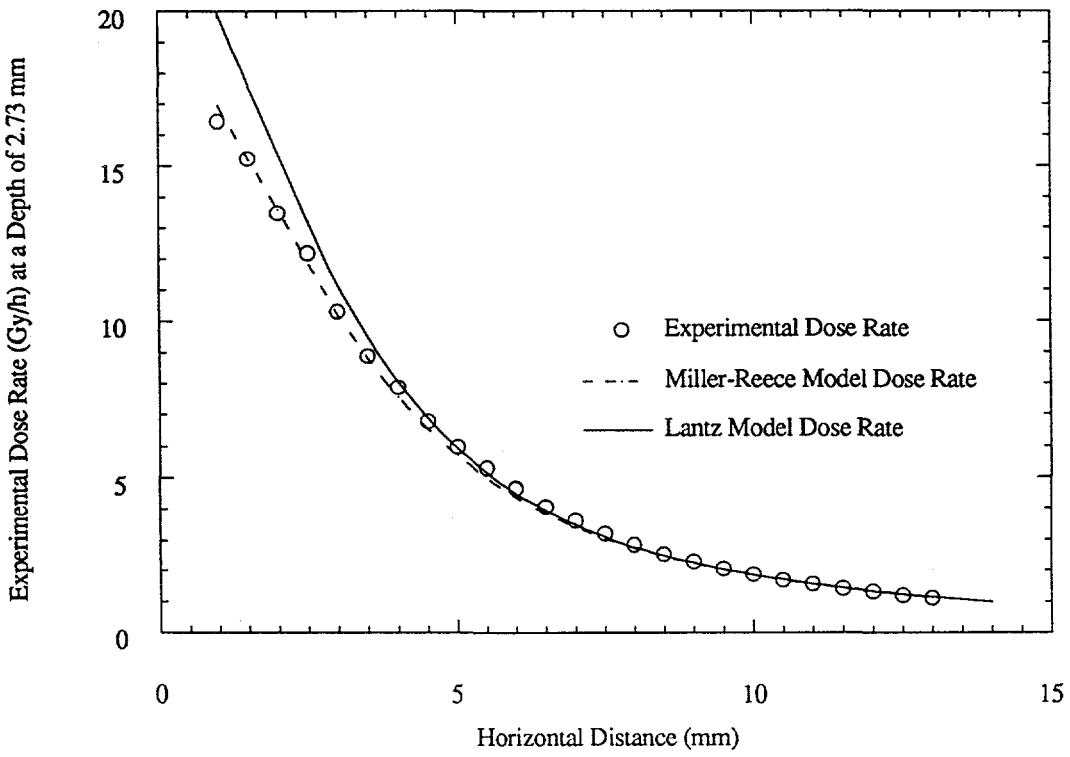

Fig. 16. A comparison of measured and modeled dose rates for the ^{60}Co hot particle.

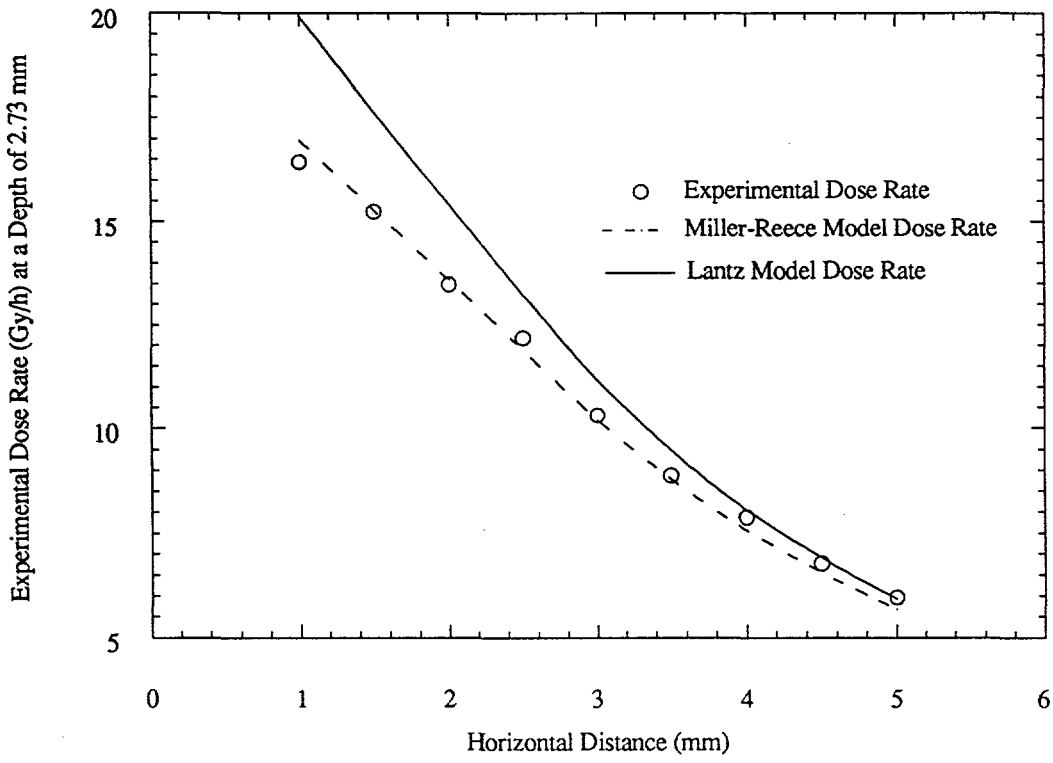

Fig. 17. An expanded view of the comparison between measured and modeled dose rates for the ^{60}Co hot particle.

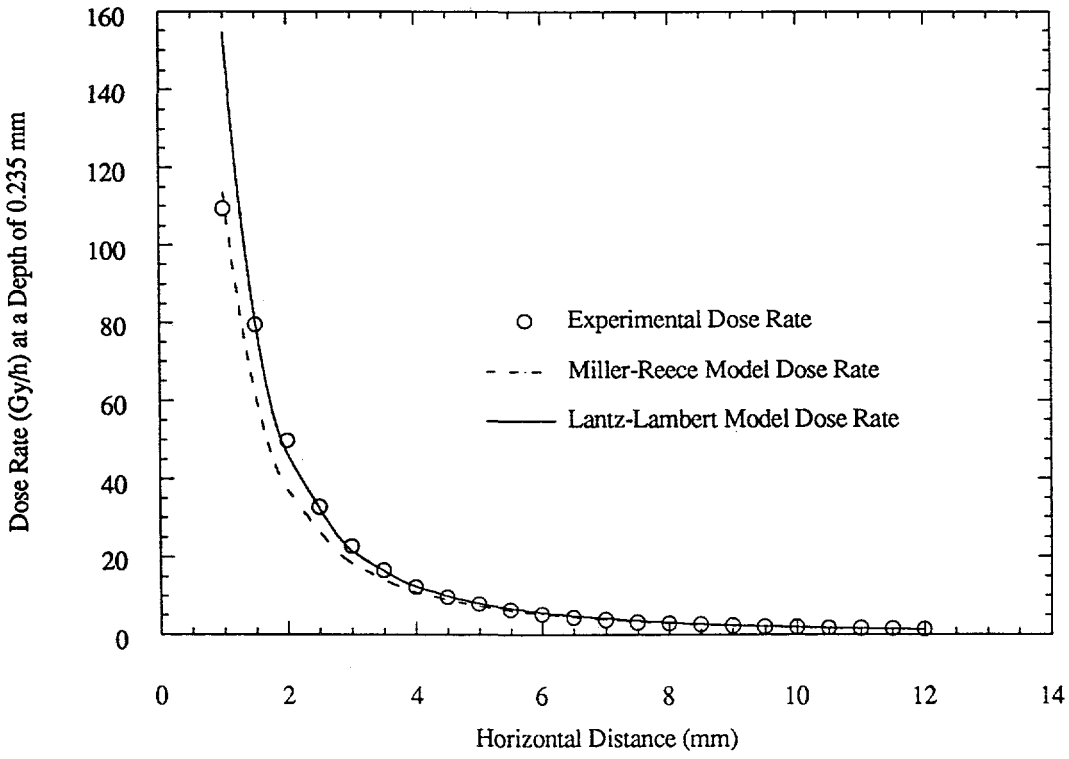

Fig. 18. A comparison of measured and modeled dose rates for a shallow exposure.

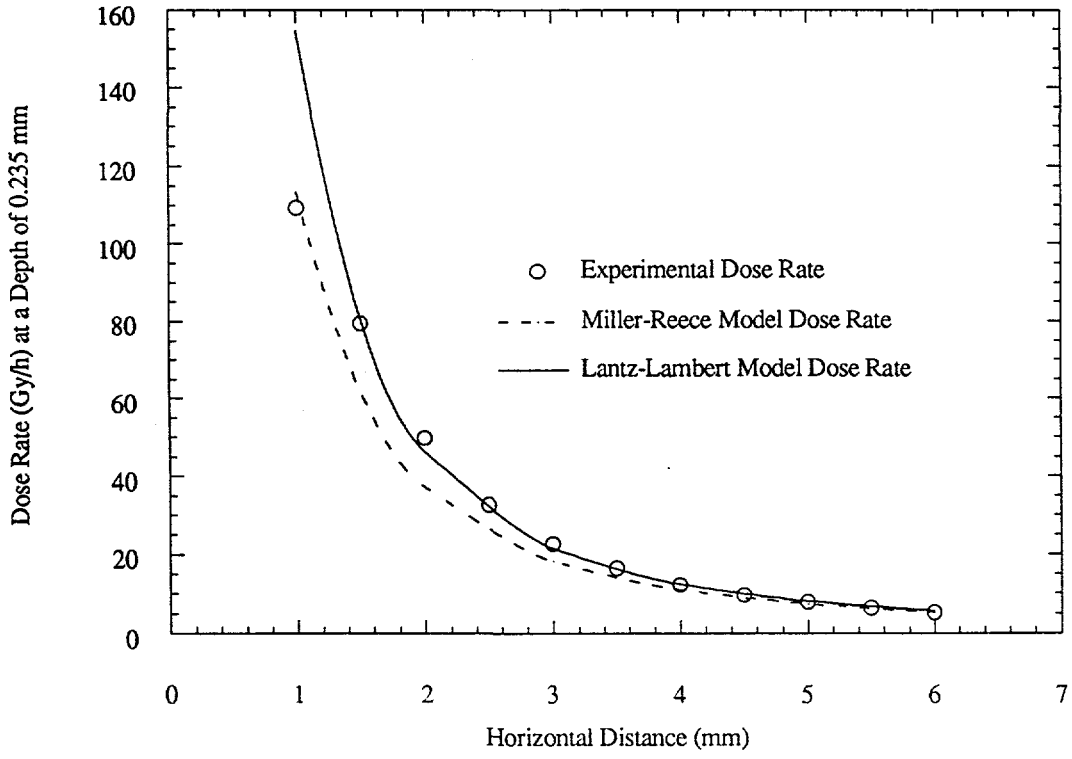

Fig. 19. An expanded view of the comparison between measured and modeled dose rates for a shallow exposure.

emphasize the correlation between the experimental data and the Miller-Reece model predictions. A correlation coefficient of 0.999 was calculated for the Miller-Reece model and the deep exposure data. The Miller-Reece model has a correlation coefficient of 0.991 for the shallow exposure data. The Lantz-Lambert model has a correlation coefficient of 0.655 for the deep exposure data and 0.988 for the shallow exposure data. The Lantz-Lambert model agrees with the experimental data under CPE conditions but overestimates dose when CPE does not exist. The favorable comparisons with the Miller-Reece model lend confidence that the experimental dose measurements accurately assess the degree of CPE achieved at a given depth.

This is the first time that measurements have been published to test the CPE models. Further research is needed to determine the accuracy of the models for exposures to gamma rays with various energies. A ^{137}Cs exposure would provide valuable data with which to test these models.

REFERENCES

Attix, Frank H. Introduction to radiological physics and radiation dosimetry. First printing. New York: John Wiley and Sons: 1986.

Chabot, George E. The physics and determination of absorbed dose associated with external beta radiation exposures. Unpublished article. University of Lowell. Lowell, MA. 1990.

Durham, J. S. and Lantz, M.W. Determination of gamma absorbed dose rates and charged particle equilibrium from hot particles. Radiat. Prot. Management. 8:35-41; 1991.

GAF Chemicals Corporation. GAF product information and calibration kit, brochure 2304-005. Coleta, CA. 1990.

Health Physics and Radiological Health Handbook, The. 1st. ed. Silver Spring, MD.: Scinta, Inc.: 1992.

Hine, G. J. and Brownell, G. L. Radiation dosimetry. New York. Academic Press Inc. 1956.

Lantz, M.W. and Lambert, M. W. Charged particle equilibrium corrections for the gamma component of hot particle skin doses. Radiat. Prot. Management. 7:38-48; 1990.

McLaughlin, W. L., Miller, A., Uribe, R. M., Kronenburg, S. and Siebentritt, C. R. Energy dependence of radiochromic dosimeter response to X and gamma rays. In high dose dosimetry, proceedings of an International Atomic Energy Agency Symposium. Vienna: IAEA; IAEA-SM-272/9; 1984: 39-424.

Miller, S. D. and Reece, W. D. Electronic non-equilibrium effects on dose to the basal layer of the skin from gamma emitting contamination. Presented at the Thirty-fifth annual meeting of the Health Physics Society. Anaheim, CA. 1990.

Saylor, M.C., Tamargo, T. T., McLaughlin, W. L., Khan, H. M., Lewis, D. F., and Schenfele, R. D. A thin film recording medium for use in food irradiation. Radiat. Phys. Chem. 31:529-536; 1988.

Shaw, Kimberly. Dose profiles through the dermis for both on- and off-skin hot particle exposures. A thesis for Master of Science. Texas A&M University, College Station, TX. 1993.

Soares, C. G., Coursey, B. M., McWilliams, F. F. and Scanell, M. J. Dose mapping of radioactive hot particles using radiochromic film. Radioactivity and Radiochemistry. Spring:14-16; 1990.

Traub, R. J., Reece, W. D., Scherplez, R. I. and Sigalla, L. A. Dose calculation for contamination of the skin using the computer code VARSKIN. NUREG/CR-4418 PNL-5610; 1987.

U. S. Nuclear Regulatory Commission. Excessive skin exposures due to contamination with hot particles. Inspection and Enforcement Notice 86-23, April 9, 1986.

U. S. Nuclear Regulatory Commission. Standards for protection against radiation. Washington, DC: U. S. Government Printing Office; Title 10, Chapter I, Code of Federal Regulations, Part 20 (10 CFR 20); revised as of 1 January 1986.

VITA

Jo Ann Myrick is the daughter of Mrs. Ozelle Fischer Myrick and the late Mr. Paul Myrick. She graduated from Alice High School in 1989. In May of 1993 she received a Bachelor of Science in Radiological Health Engineering from Texas A&M University. She will receive a Master of Science in Health Physics from Texas A&M University in August, 1994. While at Texas A&M, she worked at the Nuclear Science Center in the Health Physics/Laboratory Operations Department. She was appointed to the Applied Health Physics Fellowship Program administered by Oak Ridge Associated Universities for the U. S. Department of Energy in May 1993. Miss Myrick can be reached at 744 West Third Street, Alice, Texas 78332.